Earth and Planetary Science Letters 553 (2021) 116619

Contents lists available at ScienceDirect

Earth and Planetary Science Letters

www.elsevier.com/locate/epsl

Evidence for methane isotopic bond re-ordering in gas reservoirs sourcing cold seeps from the Sea of Marmara

T. Giunta [a,b,*], J. Labidi [c,d], I.E. Kohl [d,1], L. Ruffine [a], J.P. Donval [a], L. Géli [a], M.N. Çağatay [e], H. Lu [f], E.D. Young [d]

[a] IFREMER, Unité des Géosciences Marines, 29280 Plouzané, France
[b] Université de Bretagne Occidentale, Laboratoire Géosciences Océan, 29280 Plouzané, France
[c] Université de Paris, Institut de Physique du Globe de Paris, CNRS, F-75005 Paris, France
[d] University of California Los Angeles, Department of Earth, Planetary and Space Sciences, CA 90095, Los Angeles, USA
[e] Istanbul Teknik University, Faculty of Mines, Department of Geological Engineering, TR-34469 Istanbul, Turkey
[f] Peking University, Department of Energy & Sciences, College of Engineering, Beijing 100871, China

ARTICLE INFO

Article history:
Received 20 January 2020
Received in revised form 14 September 2020
Accepted 28 September 2020
Available online xxxx
Editor: L. Robinson

Keywords:
cold seeps
methane
clumped isotopologues
bond-ordering

ABSTRACT

The measurement of methane clumped isotopologues ($\Delta^{13}CH_3D$ and $\Delta^{12}CH_2D_2$) allows exploring isotope bond ordering within methane molecules, and may reveal equilibrium temperatures. Whether such temperature reflects the formation or re-equilibration temperature of the methane is not well understood, but would have critical implications for the use of methane clumped isotopologues as geo-thermometers. Here we investigate gas bubbles from vigorous emissions at cold seeps (n = 14) in the Sea of Marmara, Turkey. These cold seeps are sourced from deeper sedimentary reservoirs. Conventional geochemical tracers such as carbon and hydrogen bulk isotopic ratios ($^{13}C/^{12}C$ and D/H) or *n*-alkane molecular ratios, suggest these gases reflect various degrees of mixing between thermogenic and microbial sources. Some samples would generally be considered purely microbial in origin ($C_1/C_{2+} > 1500$; $\delta^{13}C < -60‰$). We report measurements of $\Delta^{13}CH_3D$ and $\Delta^{12}CH_2D_2$ showing that a fraction of those gases are in internal thermodynamic equilibrium, with the abundances of the two mass-18 isotopologues indicating concordant temperatures of ~90 °C and ~130 °C. These concordant temperatures are recorded by gases of putative microbial and thermogenic origin; the temperatures of equilibration are irrespective of the formation mechanism of the gases. We conclude that the two high-temperatures recorded by $\Delta^{13}CH_3D$ and $\Delta^{12}CH_2D_2$ are best explained by non-enzymatic re-equilibration at two local subsurface temperatures. First principles suggest that unequal rates of exchange are possible. Disequilibrium signatures where the two isotopologues yield discordant apparent temperatures are exhibited by other samples. In those cases the data define a trend of variable $\Delta^{13}CH_3D$ at nearly constant $\Delta^{12}CH_2D_2$. These signatures are enigmatic, and we investigate and reject multiple possible explanations including mixing, diffusion or Anaerobic Oxidation of Methane. Different rates of re-equilibration between the two rare isotopologues are implied, although lacks experimental foundation at present. In general, all of these data point towards re-equilibration of the mass-18 methane isotopologues as an important process.

1. Introduction

In most natural settings, the generation of hydrocarbon gases results from the degradation in the subsurface of organic-rich sedimentary horizons, either through thermocatalytic cracking (i.e. referred as thermogenic generation), or through microbial reduction of oxidized carbon-bearing species (i.e. microbial methanogenesis). Geochemical investigations of methane and other light hydrocarbons have historically been undertaken using bulk stable isotope ratios of carbon and hydrogen ($\delta^{13}C$ and δD), as well as molecular ratios of light *n*-alkanes (e.g. Bernard et al., 1976; Schoell, 1988). For example, thermogenic gases are expected to contain methane and variable (but significant) amount of C_{2+} gases (i.e. non-methane *n*-alkanes), with $\delta^{13}C$ and δD values evolving as a function of the thermal maturity (Schoell, 1988; Tang et al., 2000) whereas microbial gases are overwhelmingly composed of

* Corresponding author at: IFREMER, Unité des Géosciences Marines, 29280 Plouzané, France.
E-mail address: thomas.giunta@ifremer.fr (T. Giunta).
[1] Now at Thermo Fisher Scientific (Bremen) GmBH, Hanna-Kunath Str. 11 28199, Bremen, Germany.

https://doi.org/10.1016/j.epsl.2020.116619
0012-821X/

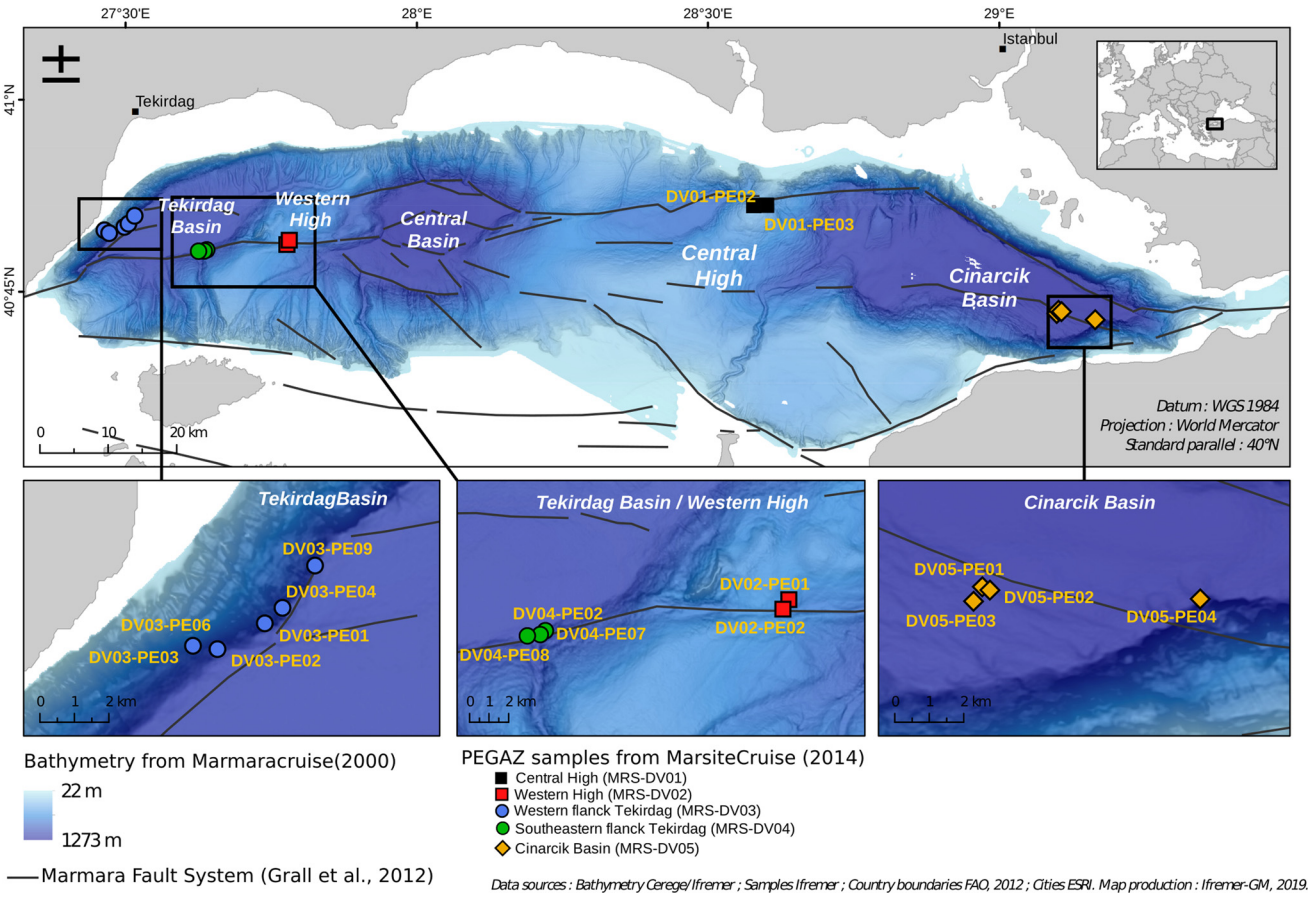

Fig. 1. Map of the Sea of Marmara showing the location of the five ROV dives (DV) and gas sampling locations. (For interpretation of the colors in the figure(s), the reader is referred to the web version of this article.)

methane (Martini et al., 1998) with $\delta^{13}C$ and δD being generally lower than methane of thermogenic origin.

Recent advances in high-resolution mass-spectrometry and in laser absorption spectroscopy have allowed the measurement of the relative abundances of doubly-substituted methane isotopologues (i.e. methane molecules containing two heavy isotope substitutions) $^{13}CH_3D$ (Stolper et al., 2014a; Ono et al., 2014; Young et al., 2016) and $^{12}CH_2D_2$ (Young et al., 2016; Eldridge et al., 2019; Gonzalez et al., 2019). These abundances are usually reported as per mil deviations from the "stochastic" isotopologue abundances that would occur with random distributions of isotopes across all species, $\Delta^{13}CH_3D$ and $\Delta^{12}CH_2D_2$. This novel approach allows the investigation of isotope bond ordering in methane molecules. At thermodynamic equilibrium $\Delta^{13}CH_3D$ and $\Delta^{12}CH_2D_2$ provide independent measurements of temperature of formation or equilibration. Where the two temperatures do not agree, kinetic processes or mixing is implied.

Rare mass-18 methane isotopologues have been shown to provide apparently reliable formation temperatures in numerous natural settings, from thermogenic (Stolper et al., 2014b, 2015; Wang et al., 2015; Douglas et al., 2016; Young et al., 2017; Giunta et al., 2019), to hydrothermal (Wang et al., 2015, 2018) and even possibly to some microbially-dominated settings (Stolper et al., 2015; Wang et al., 2015; Inagaki et al., 2015). Yet, the idea that methane 'clumped' isotopes would reflect the formation temperature requires that methane is synthesized at thermodynamic equilibrium. This later requirement is puzzling because methane generation, whether thermogenic, microbial or abiotic, is always considered to be controlled by kinetic effects rather than by thermodynamic equilibrium (e.g. Berner and Faber, 1996; McCollom, 2013). In the laboratory, the role of kinetic isotope effects on clumped isotopes is clear, especially for microbial generation, and laboratory experiments generally yield disequilibrium signatures (Stolper et al., 2015; Wang et al., 2015; Douglas et al., 2016; Young et al., 2017; Shuai et al., 2018; Gruen et al., 2018; Giunta et al., 2019), belying temperature information. Note that these disequilibrium signatures associated with microbial or low-temperature abiotic methane are also observable in nature, especially when measurements of both $\Delta^{13}CH_3D$ and $\Delta^{12}CH_2D_2$ are combined (Young et al., 2017; Giunta et al., 2019). In contrast, thermogenic methane in sedimentary basins seems to show evidence for equilibrium relative abundances of CH_4 isotopologues (Young et al., 2017; Giunta et al., 2019) and it is unclear whether this could reflect a formation temperature or a re-equilibration that occurred after formation.

In this study, we investigate methane emitted from vigorous free-gas vents at cold seep sites in the Sea of Marmara (SoM, see Fig. 1) (Géli et al., 2008; Bourry et al., 2009; Ruffine et al., 2018a). These vents are sourced by underlying sedimentary reservoirs (Ruffine et al., 2018b; Géli et al., 2018). Combining gas composition with carbon and hydrogen stable isotope analyses, two main origins of gas were identified (Ruffine et al., 2018b). Gases sampled on the structural highs, the Western High and Central High, are thought to be thermogenic in origin, whereas gases sampled in the southern flank of the Tekirdağ Basin and in the Çinarcik Basin are thought to be essentially microbial in origin. Other gases from the area were interpreted to reflect various proportions of mixing between these two types of sources. Hydrate formation or destabilization is unlikely to have affected these gases. All gases were collected at locations where thermodynamic conditions for hydrate stabilization are not met with the exception of samples collected in the Western High (Ruffine et al., 2012, 2018b). In contrast, the chemical and isotopic compositions have been all ac-

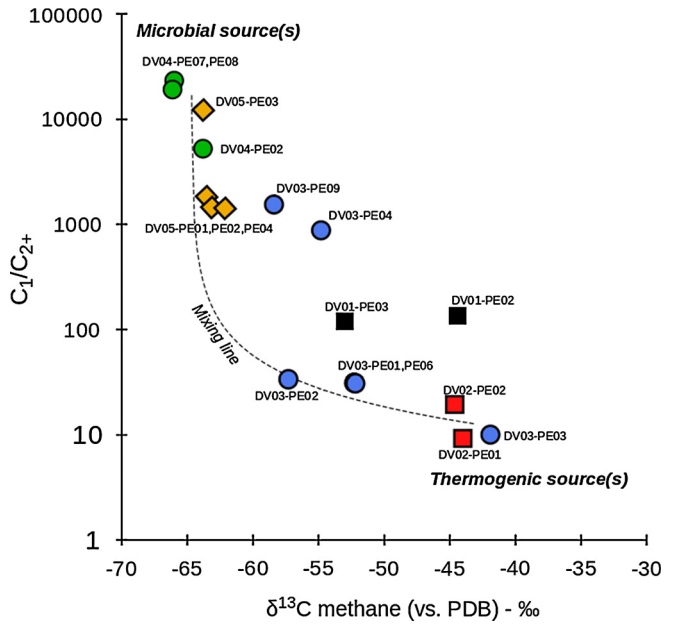

Fig. 2. 'Bernard plot' (Bernard et al., 1976): the wetness gas ratio $C_1/(C_2+C_3+C_4)$, is reported as a function of the methane $\delta^{13}C$, together with a hypothetical two-endmembers mixing curve. Data reported here are the same as used in Ruffine et al. (2018b).

counted for by mixing. Mixing as illustrated in Fig. 2 using the methane $\delta^{13}C$ versus C_1/C_{2+} ratios (Ruffine et al., 2018b). Thermogenic gases are typically thought to contain significant amounts of C_{2+} gases and therefore to show low C_1/C_{2+} ratios together with relatively enriched methane $\delta^{13}C$ values (e.g. Bernard et al., 1976). In contrast, microbial gases are expected to be dominated by methane with trace amounts of C_{2+} gases and are therefore expected to have high C_1/C_{2+} ratios together with relatively low $\delta^{13}C$ values. Thus, mixing between thermogenic and a microbial end members is predicted to produce a characteristic mixing hyperbola (Fig. 2). Some samples from the SoM however – especially gases from the Central High and from the western flank of the Tekirdağ Basin – appear to deviate from this mixing line. These gases were noted to show anomalously heavy propane $\delta^{13}C$ (Ruffine et al., 2018b), comprising evidence for biodegradation of propane (James and Burns, 1984) which could explain the departure from the two endmembers mixing line (Fig. 2). In this study, we explore further these hypotheses by combining the measurement of $^{13}CH_3D$ and $^{12}CH_2D_2$ to provide additional constraints on the thermal history of methane in the sedimentary reservoirs feeding the Marmara cold vents.

2. Geological setting and fluid activity

The Sea of Marmara (SoM) is an interior sea located in the Turkish territory and links the Black sea to the northeast and the Mediterranean sea to the west via the Bosphorus and the Darnaelle straits, respectively. The SoM is composed of three basins, the Tekirdağ Basin, the Central Basin and the Çınarcık Basin, which latter reaches a maximum depth of 1273 m. Each of the basins are separated by push-up structures, the Western High and the Central High (see Fig. 1). The SoM seafloor is cut lengthwise by a dense network of faults belonging to the North Anatolian Fault (NAF) system which accommodates the slip motion between the Eurasian plate and the Anatolian block (e.g. Armijo et al., 2000). In the northern part of this network, the Main Marmara Fault is seismically the most active sequence of fault segments in the region, having caused devastating earthquakes in the past (e.g. Ambraseys and Jackson, 2000).

At the seafloor, cold seeps with fluid and gas emissions are widespread across the SoM, but appear to be more frequent near active faults (e.g. Géli et al., 2008), perhaps suggesting a relationship between pressurized gas reservoirs and seismic activity (Gasperini et al., 2011; Géli et al., 2018). The sampling of free-gas (i.e. bubbles) emanating at the SoM seafloor was first achieved during the Marsite cruise in 2007, after detection of gas seep locations using a SIMRAD-EK60 echo sounder and acoustic anomalies associated to gas bubbles in the water column (Géli et al., 2008). At the time, only three active gas sites were sampled in the Çinarcik Basin, in the Western High and in the Central High (Bourry et al., 2009). In 2014, a more extensive study on gases discharged at the SoM seafloor along the NAF was undertaken during the Marsite Cruise (Ruffine et al., 2018a,b). Through combination of acoustic survey and ROV dives, new active sites were discovered and sampled in the Çinarcik Basin, in the Western High and in the Central High, as well as in the Tekirdağ Basin (Ruffine et al., 2018b). Gases that are venting at the seafloor consist mainly of methane-rich mixtures (up to >99%-mol), some of which containing significant amount of other hydrocarbon. The contribution of light *n*-alkanes is thought to reflect hydrocarbon formation within sediments in the SoM via organic matter degradation, both thermocatalytic cracking of organic matter and microbial reduction of oxidized carbon-bearing species have been suggested (Gürgey et al., 2005; Ruffine et al., 2018b).

3. Methods

Gas samples were collected in the course of the Marsite Cruise in November 2014. Method for gas sampling and preservation are outlined in details in Ruffine et al. (2015, 2018b). Seafloor gas vents were identified by coupling water column acoustic guiding and visual inspection with the ROV Victor 6000. The most vigorous gas vents were then sampled with the PEGAZ sampler, a sampling device manipulated by the ROV which is designed to sample gas bubbles and preserve them at *in situ* pressure. Gas aliquots were then sub-sampled at pressure ranging between 2 and 4 bars in 12 mL Labco vials. These Labco vials were then used for measuring the gas composition (light alkanes, N_2 and CO_2 contents) as well as bulk isotope geochemistry ($\delta^{13}C$, δD) on light alkane (including methane). All these isotope analyses were performed at ISOLAB in the Netherlands. Results were reported and discussed by Ruffine et al. (2018b).

Methane gas samples were purified and analyzed at UCLA to obtain methane isotopologue abundances. The ratios $^{13}CH_3D/^{12}CH_4$, $^{12}CH_2D_2/^{12}CH_4$, $^{13}CH_4/^{12}CH_4$, and $^{12}CH_3D/^{12}CH_4$ are measured with the prototype Nu Instruments Panorama, a high-resolution gas-source double-focusing mass spectrometer at UCLA. Mass-18 isotopologue compositions are reported versus a stochastic distribution (Wang et al., 2004), representing a theoretically infinite temperature, and expressed in per mil using the capital delta notation:

$$\Delta^{13}CH_3D = [(^{13}CH_3D/^{12}CH_4)_{sample}/(^{13}CH_3D/^{12}CH_4)_{stochastic} - 1] \times 1000 \quad (1)$$

and

$$\Delta^{12}CH_2D_2 = [(^{12}CH_2D_2/^{12}CH_4)_{sample}/(^{12}CH_2D_2/^{12}CH_4)_{stochastic} - 1] \times 1000. \quad (2)$$

Methods for sample purification and isotope ratio measurements are outlined in detail by Young et al. (2016, 2017) and briefly summarized here. Prior to measurements of isotopologues, methane is

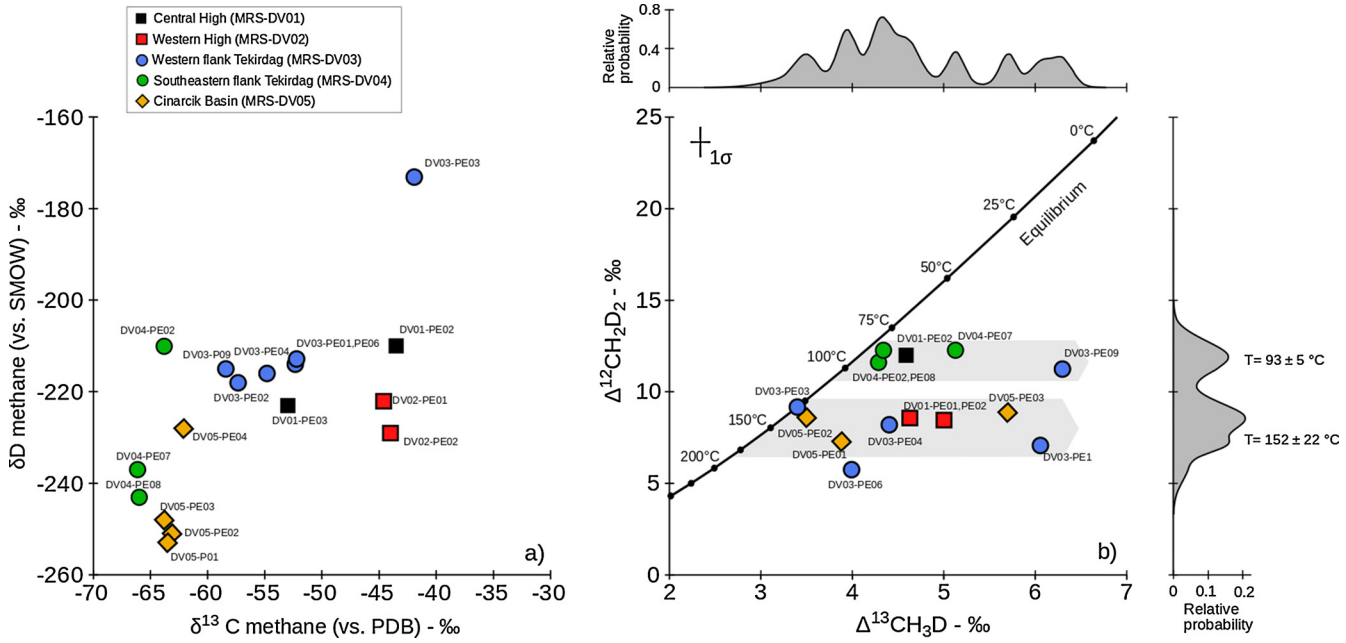

Fig. 3. a) Methane bulk isotope composition. $\delta^{13}C$ and δD measured on the Panorama are within uncertainty of these measurements. b) Methane isotopologue composition for SoM gas samples. The relationship between $\Delta^{13}CH_3D$ and $\Delta^{12}CH_2D_2$ and temperature is calculated following Young et al. (2016, 2017), see details in the Appendix. Despite the disagreement between the temperatures calculated for most samples, the distribution of $\Delta^{12}CH_2D_2$-based temperatures appear to be bi-modal, averaging at $93 \pm 5\,°C$ and $152 \pm 22\,°C$, with few samples matching these temperatures for $\Delta^{13}CH_3D$ as well. Note these two apparent temperatures roughly match the maximum temperatures reached by two of the main source rocks (i.e. organic-rich sediments) in the area, the Eocene Hamitabad Formation and the Oligocene Mezardere Formation (Huvaz et al., 2005; Gürgey, 2009).

purified on a vacuum line interfaced with a gas chromatograph (GC). Two GC columns are coupled in series using He as the carrier gas. The first column consists of a 3-m long, 1/8-inch OD stainless steel tubing, packed with 5A molecular sieve and is used to separate H_2, Ar, O_2 and N_2 from CH_4 and other alkanes. The second column is used to separate CH_4 from other hydrocarbons and consists of a 2-m long 1/8-inch OD stainless steel tubing packed with HayeSep D porous polymer. Peaks are identified on a passive TCD. In order to measure $^{12}CH_4^+$, $^{13}CH_4^+$, $^{12}CH_3D^+$, $^{13}CH_3D^+$ and $^{12}CH_2D_2^+$ ion currents, the mass spectrometer is set to a mass resolving power equal to or greater than 40000. This allows resolving of the two mass-18 isotopologues ($^{13}CH_3D$ and $^{12}CH_2D_2$), both measured on the axial collector with an electron multiplier. Meanwhile, mass-16 and mass-17 isotopologues are measured on Faraday collectors with amplifier resistors of 10^{11} Ω. Sample and reference bellows are adjusted so that ion current intensities are balanced. The current intensities are rebalanced after each measurement cycle. At first, the magnet is set to measure simultaneously $^{12}CH_3D^+/^{12}CH_4^+$ and $^{12}CH_2D_2^+/^{12}CH_4^+$ ratios, with $^{12}CH_2D_2^+$ (18.04385 amu) being measured on the axial collector. In a second setting, the magnet is set to measure $^{13}CH_3D^+$ (18.04090 amu) on the axial collector, and $^{13}CH_4^+/^{12}CH_4^+$ and $^{13}CH_3D/^{12}CH_4^+$ ratios are measured simultaneously. Overall, the external 1σ error ($n = 5$) including both the accuracy and the reproducibility is estimated to be ±0.1‰ for $\Delta^{13}CH_3D$, ±0.8‰ for $\Delta^{12}CH_2D_2$, ±0.1‰ for $\delta^{13}C$, and of approximately ±0.3‰ for δD. Note that the measurements of methane $\delta^{13}C$ and δD values performed conjointly with the rare methane isotopologues are within uncertainties of measurements previously performed at ISOLAB.

4. Results

The measurements of $\Delta^{13}CH_3D$ and $\Delta^{12}CH_2D_2$ allow the description of methane isotopic bond-ordering in a given sample. At thermodynamic equilibrium both $\Delta^{13}CH_3D$ and $\Delta^{12}CH_2D_2$ should be concordant in recording the same temperature of equilibrium. The data are shown in Fig. 3, together with the theoretical thermodynamic equilibrium curve (Young et al., 2016). Samples DV04-PE02, DV04-PE08, DV01-PE02, DV03-PE03 and DV05-PE02 appear close to equilibrium, though they show two populations of $\Delta^{13}CH_3D$ and $\Delta^{12}CH_2D_2$ values (Fig. 3b). The first group composed of samples DV03-PE03 and DV05-PE02 define average $\Delta^{13}CH_3D$ and $\Delta^{12}CH_2D_2$ values of 3.45 ± 0.1‰ and 8.88 ± 0.4‰ yielding apparent concordant temperatures of 127^{+5}_{-5} °C and 135^{+7}_{-7} °C, respectively. These consistent temperatures are indistinguishable, and suggest that isotope ordering was in response to thermodynamic equilibrium in these samples. The second group composed of samples DV01-PE02, DV04-PE02 and DV04-PE08, define average $\Delta^{13}CH_3D$ and $\Delta^{12}CH_2D_2$ of 4.40 ± 0.16‰ and 11.96 ± 0.32‰, yielding nearly concordant apparent temperatures of 77^{+7}_{-8} °C and 92^{+4}_{-4} °C, respectively. The remaining samples appear shifted to the right of the equilibrium curve to varying degrees, i.e. they show higher $\Delta^{13}CH_3D$ values at a given $\Delta^{12}CH_2D_2$ relative to equilibrium (Fig. 3b). For these, it is not clear whether any temperature information can be *a priori* obtained from either $\Delta^{13}CH_3D$ or $\Delta^{12}CH_2D_2$. Probability density plots indicate that the distribution of $\Delta^{12}CH_2D_2$ values is bi-modal (Fig. 3b), with peaks at 8.01 ± 1.08‰ and 11.88 ± 0.44‰, corresponding to apparent temperatures of 152 ± 22 °C and 93 ± 5 °C, respectively. These two temperatures are remarkably similar to maximum temperatures reached by two main source rocks in the area, the Eocene Hamitabad Formation and the Oligocene Mezardere Formation (Huvaz et al., 2005; Gürgey, 2009).

Samples from the western flank of the Tekirdağ Basin (DV03) may be taken as a telling illustration of the overall complexity of our dataset. These gases show the widest variability in methane doubly-substituted isotopologue signatures, with $\Delta^{13}CH_3D$ ranging from 3.4 to 6.3‰, and $\Delta^{12}CH_2D_2$ ranging from 5.7 to 11.2‰. These samples also show the largest variability in C_1/C_{2+} values ranging from 10 to 1560 (Fig. 2), and bulk $\delta^{13}C$ ranging from −41.2 to −58‰ (Fig. 2, Fig. 3a). However, perhaps most curious is that two samples, DV03-PE01 and DV03-PE06 are nearly identical both in

their gas composition and in their bulk isotopic signatures (Fig. 2, Fig. 3a), and yet show significantly different $\Delta^{13}CH_3D$ values at a given $\Delta^{12}CH_2D_2$, being members of the two distinct groups defined by the two peaks in $\Delta^{12}CH_2D_2$ values (Fig. 3b). This is also true for samples from the Çinarcik Basin (DV05) and, though less significant, for samples from the southeastern flank of the Tekirdağ Basin (DV04. All of these samples have been previously interpreted as dominantly microbial in origin (Ruffine et al., 2018b). In other words, we observe a decoupling between conventional tracers and clumped methane signatures.

Decoupling also appears for some samples which are distinct in gas composition and in bulk isotope signatures but are similar in the isotopologue space (Fig. 3b). The most striking cases are the DV03-PE03 (Tekirdağ Basin) and the DV05-PE02 (Çinarcik Basin) samples. They both plot on (or near) the equilibrium curve at an equivalent temperature of ∼130 °C. However, they have distinct bulk isotope compositions. Sample DV03-PE03 shows relatively high $\delta^{13}C$ (of −41.2‰) together with low C_1/C_{2+} (of 10) which could reflect a thermogenic end-member (Ruffine et al. (2018b) similar to oil-associated gases found in the Thrace Basin (Huvaz et al., 2005; Gürgey, 2009). An apparent equilibrium temperature of ∼130 °C derived from both $\Delta^{13}CH_3D$ and $\Delta^{12}CH_2D_2$ would indicate a temperature generally consistent with the typical range expected for thermogenic gas generation (Tissot and Welte, 1978). On the other hand, based on the lack of C_{2+} ($C_1/C_{2+} = 1456$) and low $\delta^{13}C$ and δD values −63‰ and −251‰ respectively, sample DV05-PE02 appears microbial in origin (i.e. derived from microbial methanogenesis). For this sample, apparent temperatures of $124^{-6\circ}_{+6}C$ and $139^{+14\circ}_{-13}C$, derived from $\Delta^{13}CH_3D$ and $\Delta^{12}CH_2D_2$ respectively, are within uncertainty of the upper temperature limit for life of ∼121 °C (Kashefi and Lovley, 2003; Takai et al., 2008).

Overall, variations observed in the $\Delta^{13}CH_3D$ and $\Delta^{12}CH_2D_2$ space do not correlate with bulk isotope ratios or in C_1/C_{2+}. This suggests that the isotope bond ordering is responding to forcings that are not obviously related to gas composition or bulk isotope ratios.

5. Discussion

5.1. Isotope-bond reordering

First studies on methane isotopologues have provided consistent observations when investigating methane of thermogenic or microbial origin. Apparent agreement between $\Delta^{13}CH_3D$-based temperatures and measured environmental temperatures, or expected formation temperatures were observed for most thermogenic gases (Stolper et al., 2014b, 2015, 2017; Wang et al., 2015; Douglas et al., 2016). In addition, concordant temperature from both $\Delta^{12}CH_2D_2$ and $\Delta^{13}CH_3D$ in the same samples supports the idea that thermogenic methane in natural settings is generally at 'bond ordering' equilibrium (Young et al., 2017; Giunta et al., 2019). Yet, the mechanism by which isotopologues reach equilibrium in nature is still unclear, as thermogenic generation is generally thought to be controlled by kinetics (e.g. Clayton, 1991; Tang et al., 2000; Stolper et al., 2017; Xia and Gao, 2019). Recently, experimental and modeling works have also shown that disequilibrium signatures could be expected during gas generation and/or accumulation in reservoirs (Shuai et al., 2018; Xia and Gao, 2019), yet it does not seem to be common in most natural settings.

On the other hand, microbial methane is associated with large isotopologue disequilibrium under laboratory conditions, often yielding negative $\Delta^{13}CH_3D$ (Wang et al., 2015; Stolper et al., 2015; Young et al., 2017; Douglas et al., 2016; Gruen et al., 2018; Giunta et al., 2019) and markedly negative $\Delta^{12}CH_2D_2$ values (Young et al., 2017; Giunta et al., 2019; Gonzalez et al., 2019) (Fig. 4). The causes of the disequilibrium are beyond the scope of this study but may include: the rate of methanogenesis (e.g. Wang et al., 2015; Stolper et al., 2015), the metabolic pathways (Giunta et al., 2019; Young et al., 2017), statistical combinatorial effects (Young et al., 2017; Cao et al., 2019; Taenzer et al., 2020), and/or quantum tunneling effects (Young et al., 2017). In natural settings, disequilibrium signatures similar to those observed in laboratory are commonly observed (e.g. Wang et al., 2015; Douglas et al., 2016; Giunta et al., 2019; Young, 2019), however, there are certain environments, such as in marine sediments, where isotopologue signatures appear closer to equilibrium with environmental temperatures (e.g. Wang et al., 2015; Stolper et al., 2015; Douglas et al., 2016; Inagaki et al., 2015; Giunta et al., 2019; Ash et al., 2019). This led some authors to propose that isotopologue signatures during microbial methanogenesis would be largely controlled by the degree of metabolic reversibility (Wang et al., 2015; Stolper et al., 2015), and may sometimes, especially in the deep biosphere, result in methane in isotopologue equilibrium. Young et al. (2017) argued that microbial communities may drive methane towards equilibrium in nature, and Young (2019) presented preliminary evidence for the potential role of methanotrophic organisms performing Anaerobic Oxidation of Methane (AOM) in re-ordering atomic bonds within methane molecules towards the equilibrium (also supported by Giunta et al., 2019). Ash et al. (2019) presented evidence that AOM causes methane to achieve equilibrium $\Delta^{13}CH_3D$ and $\Delta^{12}CH_2D_2$ values in the sediments from the Bornholm Basin, Baltic Sea. Both proposed mechanisms for equilibration lack unequivocal experimental validation at present.

In SoM gases, samples DV03-PE03 and DV01-PE02 were identified as dominantly thermogenic in origin (Ruffine et al., 2018b) and define two distinct but concordant temperatures of ∼130 °C and ∼90 °C, respectively (Fig. 3b). Both temperatures are consistent with the 'gas window' for thermogenic generation (Tissot and Welte, 1978) and with maximum temperatures reached by two main source rocks in the area, the Eocene Hamitabad Formation and the Oligocene Mezardere Formation (Huvaz et al., 2005; Gürgey, 2009). We therefore interpret these data as recording characteristic regional temperatures for methane equilibration.

In contrast, samples DV05-PE02, DV04-PE02 and DV04-PE08 are considered to be dominantly microbial in origin on the basis of $\delta^{13}C < -60$‰ and $C_1/C_{2+} > 1000$, but nonetheless plot on (or near) the equilibrium curve at temperatures of ∼90 and ∼130 °C, the same two temperatures recorded by the thermogenic samples (Fig. 3b). It is unlikely that these relatively high temperatures for nominally microbial gases are the result of hyper-thermophilic activity in sediments of the SoM. A temperature of ∼130 °C slightly exceeds the upper temperature limit for life of 121 °C, a maximum that has so far only been observed for optimal laboratory conditions and for archeal strains that are typical of energy-rich hydrothermal vent environments (Kashefi and Lovley, 2003; Takai et al., 2008). The temperature limit for microbial degradation of organic matter in subsurface sedimentary settings that are nutrient-starved systems is considered to be 80-90 °C (Head et al., 2003), and possibly even lower at ∼60 °C in deeply buried sediments (Inagaki et al., 2015). For these reasons, we conclude that an equilibrium temperature of ∼130 °C for natural methane with microbial traits must necessary reflect a 'non-enzymatic' (i.e. abiotic) re-equilibration to a temperature reached during sediment burial, rather than the actual temperature of formation of microbial methane in the subsurface. This explanation may also hold true for putative microbial methane equilibrated at temperatures of ∼90 °C (DV04-PE04 and DV04-PE08). The implication is that the production and accumulation of microbial methane occurred prior to burial, after which it re-equilibrated upon the heating that attended burial. Accordingly, we this can not exclude that thermogenic gases now appearing on the equilibrium $\Delta^{12}CH_2D_2$ vs. $\Delta^{13}CH_3D$ curve have inherited their equilibrium signature from a

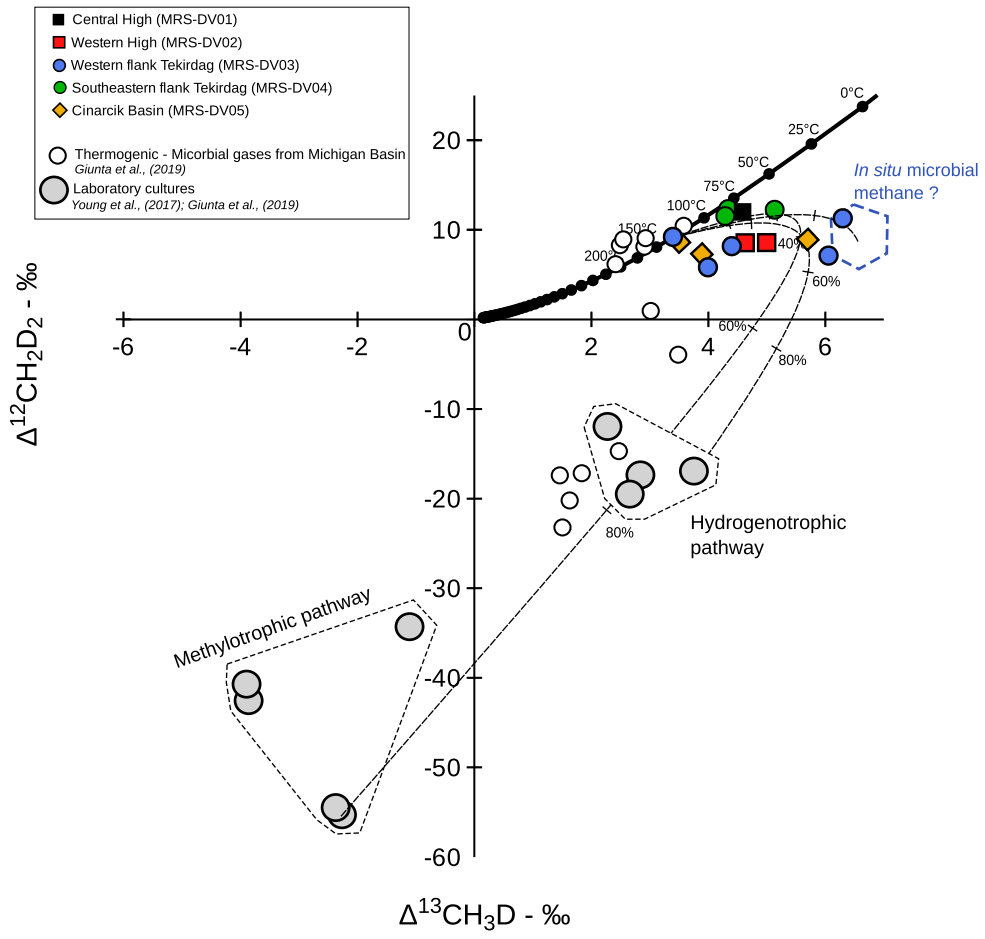

Fig. 4. Methane isotopologue signatures produced by various strains of methanogens using different metabolic pathways (see details in Young et al., 2017; Giunta et al., 2019), shown with gases from the Sea of Marmara (this study) and with thermogenic-microbial gase mixtures from the Michigan Basin (Giunta et al., 2019). Culture of methanogens in laboratory have certainly not explored the whole variability of $\Delta^{13}CH_3D$ and $\Delta^{12}CH_2D_2$ values that can be obtained during microbial generation. Potential mixing curves are given as illustrations, assuming microbial end-members at the SoM are similar to those measured in laboratory. Note that mixing may result in non-linearity effects in the $\Delta^{13}CH_3D$-$\Delta^{12}CH_2D_2$ space (Young et al., 2016; Douglas et al., 2016), with a curvature depending on bulk isotopic compositions ($\delta^{13}C$ and δD) of end-members. With this simple exercise, it is shown that if attempting to fit SoM data with a mixing line having a microbial end-member similar to those measured in laboratory, then SoM gases would at most contain 60% microbial methane which seems inconsistent with extreme C_1/C_{2+} enrichment (>1000). Instead, the data would suggest an in situ microbial end-member with a $\Delta^{13}CH_3D$ of at least 6‰, in line with other observations of microbial methane in the deep biosphere (Wang et al., 2015; Inagaki et al., 2015; Ash et al., 2019).

similar re-equilibration mechanism, rather than from their actual formation.

Rates for re-equilibration of $^{13}CH_3D/^{12}CH_4$ and $^{12}CH_2D_2/^{12}CH_4$ isotopologue ratios, especially at relatively low temperatures, are unknown. Wang et al. (2018) have speculated that rates for re-equilibration of $^{13}CH_3D$ may follow the rates for 'external', or inter-species re-equilibration of D/H ratios between methane and water in hydrothermal systems. They extrapolated from a small body of experimental data at 200, 323 and 400 °C that the timescale for CH_4 isotopic bond re-ordering in the absence of a metal catalyst would be on the order of 10^9 years for temperature of 150 °C, and $>10^{10}$ years below 100 °C. This would suggest that the relative abundances of methane isotopologues are not subject to resetting in most sedimentary settings. This conclusion appears to be contradicted by our observations. In fact, our dataset argues in favor of faster isotopologue re-ordering rates than those for inter-species isotope exchange with environmental (reservoir) waters. Our data requires that methane re-equilibration at rather cool (<150 °C) subsurface conditions can occur, promoted or catalyzed by a mechanism that remains to be identified. Recently, a similar process was suggested to account for $^{12}CH_2D_2$ re-ordering down to 65 °C with no resolvable $^{13}CH_3D$ re-equilibration in well characterized marine hydrothermal vent fluids (Labidi et al., 2020).

From this data-set, it is clear that we cannot determine with certainty whether methane achieved bond equilibrium via exchange with other molecules. Source reservoirs are not readily accessible to sampling, precluding assessments of inter-species (e.g., CH_4 and H_2O) isotopic exchange. The fact that samples DV05-PE02 and DV05-PE03 have identical δD values, but distinct $\Delta^{13}CH_3D$ values, one at equilibrium based on concordance with $\Delta^{12}CH_2D_2$, and the other not, may indicate that re-equilibration among methane molecules can occur without significant isotope exchange with other molecular species that would cause shifts in the methane bulk δD values. The alternative is that these two samples have reached D/H equilibrium with the same source of hydrogen but did not reach mass-18 isotopologue equilibrium. In either case, it appears as though rates for bond re-equilibration and for inter-species re-equilibration are decoupled.

The probability distributions in Fig. 3b suggest that $\Delta^{12}CH_2D_2$ has experienced a greater degree of re-equilibration than $\Delta^{13}CH_3D$. We investigate the prospects for this in greater detail in Section 5.2.4. The catalysis of hydrogen isotope exchange among alkanes has been studied for almost a century (see recent review by Sattler, 2018), but remains poorly understood for temperatures and timescales that might be relevant for geological applications. Transition metals are well known to catalyze hydrogen exchange

with methane (Horibe and Craig, 1995) and have been shown to promote isotopologue equilibrium at temperatures above 150 °C (Stolper et al., 2014b; Ono et al., 2014; Young et al., 2016). Recent studies have also demonstrated the potential of aluminum oxide (in the form of γ-alumina) in promoting re-equilibration of methane to temperatures as low as 1 °C (Wang et al., 2018; Eldridge et al., 2019). In both cases, it is not clear how this type of catalysis can be relevant to sedimentary environments. Alternatively, exchange mediated by clay mineral surfaces might be a process to consider, as clays are known to promote hydrogen exchange on larger organic molecules (Alexander et al., 1982; Sessions et al., 2004).

5.2. Departures from equilibrium

5.2.1. Mixing

Methane samples that do not record concordant temperatures of ~90 and ~130 °C exhibit variable but significant degrees of disequilibrium, all plotting to the right of the equilibrium curve in Fig. 3b and exhibiting relatively large variations in $\Delta^{13}CH_3D$ and relatively small variations in $\Delta^{12}CH_2D_2$. Based on bulk isotope ratios and molecular ratios, these gases may have $\Delta^{12}CH_2D_2$ and $\Delta^{13}CH_3D$ values resulting from mixing between thermogenic and microbial gases (Fig. 2; Ruffine et al., 2018b). However, mixing, if it occurred, may now be disguised by varying degrees of re-equilibration based on the evidence summarized in Fig. 3b. Nonetheless, vestiges of disequilibrium in isotopologue space due to mixing may persist. In general, the samples showing the largest offset from the equilibrium curve (DV03-PE01, DV03-PE09 and DV05-PE03) are considered to be dominantly microbial in origin based on bulk isotope ratios and the molecular concentrations comprising the gas. This suggests that one end-member for mixing was microbial, perhaps having $\Delta^{12}CH_2D_2$ and $\Delta^{13}CH_3D$ values characteristic of microbial methanogenesis in the laboratory and in some natural settings. The magnitude of the disequilibrium observed in our data is much less than that obtained from microbial methanogenesis in laboratory cultures (Young et al., 2017) and from samples of microbial methanogenesis origin in natural settings investigated to date where both $\Delta^{13}CH_3D$ with $\Delta^{12}CH_2D_2$ have been measured (Giunta et al., 2019; Young et al., 2017) (Fig. 4). Invoking a microbial end-member with a signature similar to those measured in the laboratory would imply that the most disequilibrated samples in this study are composed of no more than 40 to 60% microbial methane (Fig. 4). While mixing of this end-member with a thermogenic component explains the isotopologue data (Fig. 4), this relatively low fraction of microbial methane would be inconsistent with their $C_1/C_{2+} > 1000$ usually considered indicative of a nearly pure microbial origin (e.g. Bernard et al., 1976). This observation may in turn suggest that microbial methane in deep biosphere do necessarily resemble laboratory cultures (e.g. Wang et al., 2015; Stolper et al., 2015; Douglas et al., 2016; Giunta et al., 2019).

Gases from the Western High (DV02-PE01 and PE02) identified as mainly thermogenic also have disequilibrium $\Delta^{13}CH_3D$ and $\Delta^{12}CH_2D_2$ values (Fig. 3b.) while showing little evidence of a microbial contribution (low C_1/C_{2+} of ~15). Therefore, thermogenic gases may also have contributed to disequilibrium $\Delta^{13}CH_3D$ and $\Delta^{12}CH_2D_2$ values in mixtures. Deciphering the impact of mixing is exacerbated by a lack of correlation between C_1/C_{2+} and disequilibrium isotopologue signatures (Fig. 5). In any event, the $\Delta^{13}CH_3D$ and $\Delta^{12}CH_2D_2$ data from the SoM fail to follow a simple two-component mixing in which thermogenic gases with low C_1/C_{2+} ratios are mixed with microbial gases with elevated C_1/C_{2+} ratios. Mixing does not seem to be the primary cause of variable mass-18 isotopologues in these samples.

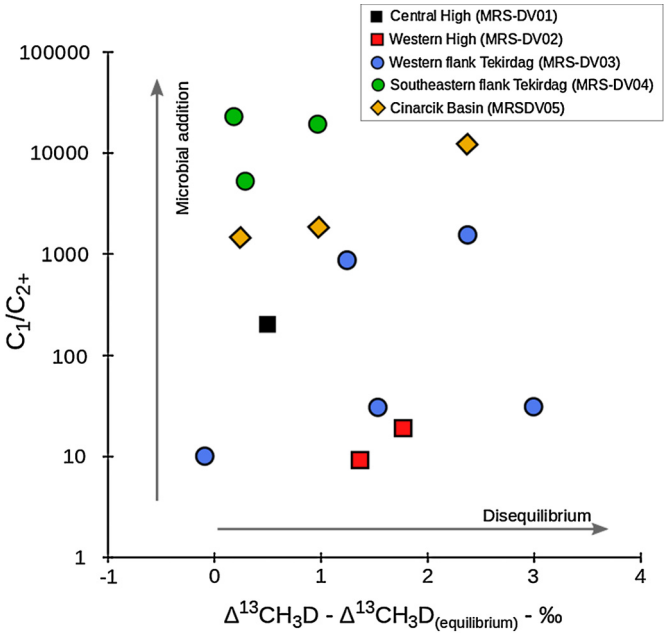

Fig. 5. Wetness ratio (C_1/C_{2+}) reported as a function of $\Delta^{13}CH_3D$-$\Delta^{13}CH_3D_{(equilibrium)}$. $\Delta^{13}CH_3D_{(equilibrium)}$ is calculated such as it matches the equivalent temperature inferred from $\Delta^{12}CH_2D_2$. This is a convenient way to evaluate for each sample, the offset from the equilibrium in the $\Delta^{13}CH_3D$-axis, and to demonstrate that there are no apparent correlation with C_1/C_{2+}. Assuming that microbial methanogenesis should produce disequilibrium, as shown in all laboratory culture experiments (Wang et al., 2015; Stolper et al., 2015; Douglas et al., 2016; Young et al., 2017; Gruen et al., 2018; Giunta et al., 2019), then in case of mixing with a microbial source, one would expect positive relationship between the two parameters.

5.2.2. Mass-dependent fractionation during migration

An alternative explanation for the disequilibrium trend of highly variable $\Delta^{13}CH_3D$ values and relatively minor variations in $\Delta^{12}CH_2D_2$ is mass fractionation of the SoM gases during their migration in the subsurface (i.e. for example from source rock to reservoir or from reservoir to reservoir) and/or to the seafloor. Though migration of free gas (bubbles) to the seafloor is an advective process and is therefore not a mechanism for fractionating isotopologues, diffusive transport prior to gas saturation can segregate methane molecules according to their masses. Diffusion favors the light isotopologues for the diffused gas (as opposed to the residual gas) resulting in decreases in $\delta^{13}C$ and δD values but increases in $\Delta^{13}CH_3D$ and $\Delta^{12}CH_2D_2$ values. In $\Delta^{12}CH_2D_2$ vs. $\Delta^{13}CH_3D$ space both axes refer to the same integer mass ratio of 18/16, and any fractionation by molecular mass, including by diffusion, should produce a 1:1 slope in this space (Young et al., 2017). A 1:1 relationship is also expected for gases affected by diffusion in δD vs. $\delta^{13}C$ space since both axes refer to integer mass ratios of 17/16. In the SoM gas samples, the slope-1 relationship expected between $\delta^{13}C$ and δD values by mass segregation according to molecular weight is only crudely evident when taken in aggregate (Fig. 6a). However, the data are more consistent with a diffusive fractionation process if one considers that $\Delta^{13}CH_3D$ and $\Delta^{12}CH_2D_2$ are distributed along two distinct diffusion trends starting from two equilibrium temperatures of about ~100 and 200 °C (Fig. 6b). These temperatures are at the high-temperature ends of the two groups of samples shown in Fig. 3b.

If diffusion is at play, samples showing the largest offset from the equilibrium curve in mass-18 isotopologue space should be relatively low in bulk $\delta^{13}C$ and δD. In detail however, when assigning self-consistent diffusion coefficients to all methane isotopologues, it appears that an enrichment of >3‰ in $\Delta^{13}CH_3D$ as observed in our data should be associated with a shift in bulk $\delta^{13}C$ by ~50‰

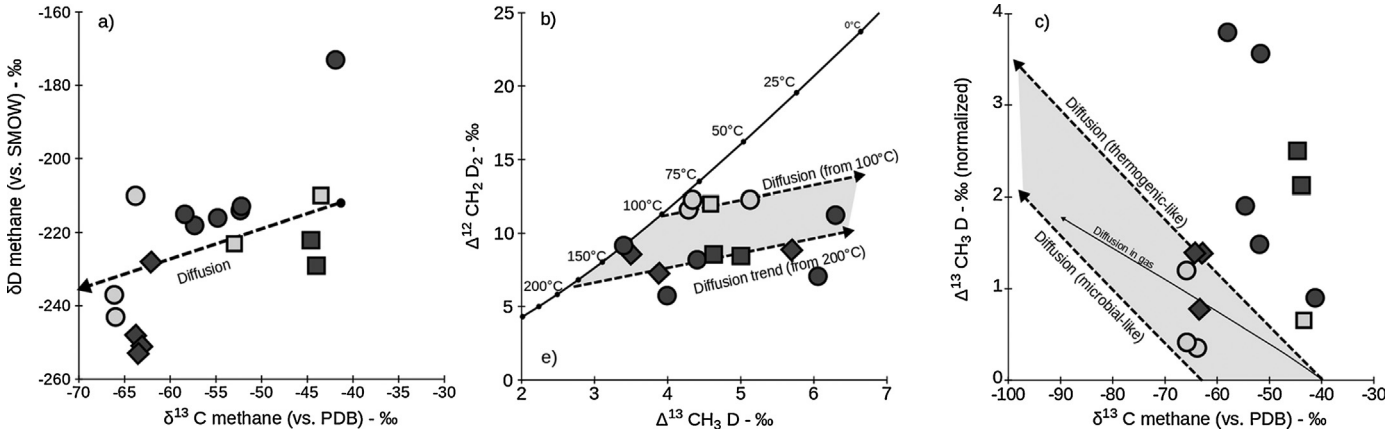

Fig. 6. Investigating the potential role of diffusion on SoM gases. Diffusion trends are plotted by solving the Fick's law in a semi-infinite space for each isotopologue. a) In a bulk δ^{13}C-δD space, diffusion should produce a 1:1 slope. b) In the $\Delta^{13}CH_3D$-$\Delta^{13}CH_3D$ space, diffusion is also expected to produce a 1:1 slope. The SoM data may suggest two distinct diffusion slopes starting at two different equilibrium temperatures of 100 °C (gray symbols) and 200 °C (dark symbols). c) $\Delta^{13}CH_3D$ as a function of bulk δ^{13}C. Note that $\Delta^{13}CH_3D$ data were normalized to their hypothetical starting equilibrium value, whether at 100 °C (grey symbols) or at 200 °C (dark symbols). The comparison of diffusive effects on singly and doubly-substituted methane isotopologues requires self consistency of diffusion coefficients assigned to each isotopologues. For singly-substituted methane isotopologues, we used $\alpha_{17\text{-}16} = D(^{13}CH_4)/D(^{12}CH_4) = D(^{12}CH_3D)/D(^{12}CH_4) = 0.997$, as determined by Prinzhofer and Pernaton (1997) for diffusion of methane in water. Following the framework of Richter et al. (2006), isotope fractionation factor associated to diffusion may be described as $\alpha_{17\text{-}16} = (17/16)^{-\beta}$, where β an empirical parameter depending on the solvent in which diffusion takes place, would thus equals to 0.05. Using this same β value for doubly-substituted isotopologues yields $\alpha_{18\text{-}16} = D(^{13}CH_3D)/D(^{12}CH_4) = D(^{12}CH_2D_2)/D(^{12}CH_4) = (18/16)^{-0.05} = 0.994$. Though not considered likely in the context of the SoM, diffusion occurring in gas phase ($\beta = 0.5$) would produce a different diffusion slope in the $\Delta^{13}CH_3D$-δ^{13}C space. In all cases, the variations observed in $\Delta^{13}CH_3D$ should be associated with much larger variations in bulk δ^{13}C than they actually are, precluding from considering diffusion as being a major process at play.

(Fig. 6c). This is not observed; our entire suite of data do not range over more than ~25‰ in δ^{13}C, so that the overall observed range of variations in $\Delta^{13}CH_3D$ appears intrinsically inconsistent with diffusion (or any mass-dependent process) being a dominant mechanism at play in the subsurface of the SoM. We conclude that diffusion is not a principal mechanism affecting the mass-18 isotopologue abundances in our methane samples.

5.2.3. Microbial methane oxidation

Apparent temperatures inferred from $\Delta^{13}CH_3D$ range from 131^{+6}_{-7} °C (DV03-PE03) to 9^{+3}_{-3} °C (DV03-PE09), perhaps representing a range from a deep reservoir temperature to a near seafloor temperature (~14 °C) if taken at face value. Thus, one may speculate that venting gases had their $\Delta^{13}CH_3D$ values re-equilibrated during their ascent towards a near-seafloor temperature, without significantly re-equilibrating $\Delta^{12}CH_2D_2$ values. Several recent studies have stressed the potential importance of microbial Anaerobic Methane Oxidation (AOM) in re-ordering isotopic bond associations in methane gas, and thus causing methane to progressively evolve towards equilibrium at ambient temperatures for both mass-18 isotopologues (e.g. Young et al., 2017; Giunta et al., 2019; Ash et al., 2019). The uptake of methane by methanotrophic organisms, in particular by archeal strains performing AOM, is a widespread process generally occurring in the first few meters of marine sediments, thus at a temperature that should not be drastically different from those at the seafloor. AOM has been recognized as a major methane sink in sediments from the SoM (e.g. Crémière et al., 2012), including in those surrounding the gas seeps studied here (Teichert et al., 2018). However, our samples were all collected as free-gas (i.e. bubbles), which is generally considered non-accessible to AOM (Luff and Wallmann, 2003; Treude et al., 2003). For AOM to have impacted the gas studied here, it would be required to have occurred prior to gas saturation. AOM is expected to yield a progressive enrichment of both δ^{13}C and δD in the residual methane (e.g. Whiticar, 1999; Holler et al., 2011), however there is no specific relationship between off-equilibrium signature and bulk signatures in our data-set (Fig. 6c may illustrate that too). In marine sediments however, AOM is expected to occur with significant reversibility effects (e.g. Yoshinaga et al., 2014), perhaps implying that a classic kinetic framework is not relevant for this type of settings. The study of methane in shallow sediments from the Bornholm Basin, Baltic Sea, yielded showed evidence for re-equilibration in $\Delta^{13}CH_3D$ and $\Delta^{12}CH_2D_2$ to environmental temperature with little effects on the bulk δ^{13}C and δD signatures (Ash et al., 2019). This study suggests that shifts in $\Delta^{13}CH_3D$ and not $\Delta^{12}CH_2D_2$, as observed in our data, being the result of AOM are unlikely.

A caveat to this conclusion arises because of preliminary experimental results suggesting that AOM under a set of restrictive conditions may yield signatures similar to our disequilibrated samples (Young, 2019). These preliminary results suggest that under low sulfate content (<1 mM), AOM mediation would re-equilibrate $\Delta^{13}CH_3D$ to environmental temperatures while maintaining the $\Delta^{12}CH_2D_2$ virtually unchanged. It is unclear how these results may be extrapolated to marine settings, but the similarity with our data-set suggests that effects on methane isotopologues due to AOM cannot be ruled out entirely. We note that the presence of a largely $\Delta^{13}CH_3D$ AOM effect driving equilibration towards colder temperatures would not be inconsistent with non-enzymatic re-equilibration as described above. The AOM would simply modify the isotopologue abundances equilibrated at ~90 and ~130 °C, prior to AOM.

5.2.4. Different re-equilibration rates for $\Delta^{13}CH_3D$ and $\Delta^{12}CH_2D_2$?

In the above sections we have discussed two mechanisms that could cause re-equilibration of methane isotopologue abundances. We suggested that non-enzymatic (i.e. abiotic) intra-methane exchange could cause re-equilibration of microbial (and perhaps thermogenic) gases formed at low temperatures to higher temperatures characteristic of known temperatures reached during sediment burial in the area (section 5.1). The bi-modal distribution of $\Delta^{12}CH_2D_2$ values suggests re-equilibration to two distinct temperatures of ~152 °C and ~90 °C that appear consistent with the thermal history of sediments beneath the SoM. Enzymatic (i.e. biotic) facilitated exchange of isotopes among methane gas molecules could have caused $\Delta^{13}CH_3D$ to partially re-equilibrate to near seafloor temperatures, perhaps during gas ascent to the seafloor (section 5.2.3). As discussed before, the bi-modal distribution of $\Delta^{12}CH_2D_2$ data seems to point towards two distinct temperatures of ~152 °C and ~90 °C that appear consistent with

the thermal history of sediments beneath the SoM. The variable $\Delta^{13}CH_3D$ data span a range of apparent temperatures from ~130 °C to ~10 °C. Based on these observations, one may speculate that our data illustrate that re-equilibration rates for the relative abundances of $^{13}CH_3D$ and $^{12}CH_2D_2$ may be different.

More specifically, the bi-modal $\Delta^{12}CH_2D_2$ values at two geologically plausible temperatures suggest isotopic bond re-ordering to equilibrium or near-equilibrium values, while $\Delta^{13}CH_3D$ values are more variable, perhaps as a result of only partial re-equilibration. This would imply that $\Delta^{12}CH_2D_2$ re-equilibrates faster than $\Delta^{13}CH_3D$, and that $\Delta^{13}CH_3D$ carries a memory of pre-reset conditions. Note this scenario does not allow the microbial methane, prior to re-equilibration, to be as low in $\Delta^{13}CH_3D$ as observed in culture studies (<4‰; e.g. Young et al., 2017) and would rather suggest a microbial methane (prior re-equilibration) with $\Delta^{13}CH_3D$ ~6‰ (equivalent to T ~ 15 °C), consistent with the idea of a deep biosphere methane being nearly equilibrated with environmental temperatures in $\Delta^{13}CH_3D$.

In order to explain our data as being purely the result of different rates of equilibration for $^{12}CH_2D_2$ and $^{13}CH_3D$, we use a simple kinetic model for exchange. In this model, we consider the intra-methane exchange reaction:

$$^{12}CH_3D + {}^{12}CH_3D \underset{k_1}{\overset{\alpha_1 k_1}{\leftrightarrows}} {}^{12}CH_2D_2 + {}^{12}CH_4 \tag{3}$$

where α_1 is the equilibrium fractionation factor and k_1 is the rate constant. A simple rate equation for this reaction is

$$\frac{d\left[^{12}CH_2D_2\right]}{dt} = \alpha_1 k_1 \left[^{12}CH_3D\right]^2 - k_1 \left[^{12}CH_2D_2\right]\left[^{12}CH_4\right] \tag{4}$$

For simplification, the concentration of $^{12}CH_4$ is set to unity ($[^{12}CH_4] = 1$), making what follows all relative to $^{12}CH_4$. We also invoke the approximation that $\alpha_1 k_1 [^{12}CH_3D]^2$ is a constant. This is justified since the concentration of $^{12}CH_2D_2$ relative to CH_4 is about 10^{-8} while that of $^{12}CH_3D$ is 10^{-4}, so $[^{12}CH_3D] \gg [^{12}CH_2D_2]$ even when working at the per mil level. In other words, we treat the change in the $[^{12}CH_2D_2]/[^{12}CH_4]$ ratio as a change in $[^{12}CH_2D_2]$ only in the rate equation. With this approximation, and some rearrangements, one obtains the solution to the differential equation as being

$$[^{12}CH_2D_2]_t = [^{12}CH_2D_2]_{EQ} + \left\{\left[^{12}CH_2D_2\right]_o - \left[^{12}CH_2D_2\right]_{EQ}\right\} e^{-k_1 t}, \tag{5}$$

where t is the time of the observation, the EQ subscript indicates equilibrium, and the o subscript indicates the initial value. Notice that as $t \to \infty$, Equation (5) reduces to $[^{12}CH_2D_2]_t = [^{12}CH_2D_2]_{EQ}$. This equation can be further rearranged into a more convenient form by dividing through by the equilibrium concentration of CH_2D_2, yielding

$$\frac{[^{12}CH_2D_2]_t - [^{12}CH_2D_2]_{EQ}}{\left[^{12}CH_2D_2\right]_o - \left[^{12}CH_2D_2\right]_{EQ}} = e^{-k_1 t} \tag{6}$$

The left-hand side of Equation (6) is the fractional approach to equilibrium. The analogous exchange reaction for $^{13}CH_3D$ is

$$^{12}CH_3D + {}^{13}CH_4 \underset{k_2}{\overset{\alpha_2 k_2}{\leftrightarrows}} {}^{13}CH_3D + {}^{12}CH_4 \tag{7}$$

and results in

$$\frac{[^{13}CH_3D]_t - [^{13}CH_3D]_{EQ}}{\left[^{13}CH_3D\right]_o - \left[^{13}CH_3D\right]_{EQ}} = e^{-k_2 t} \tag{8}$$

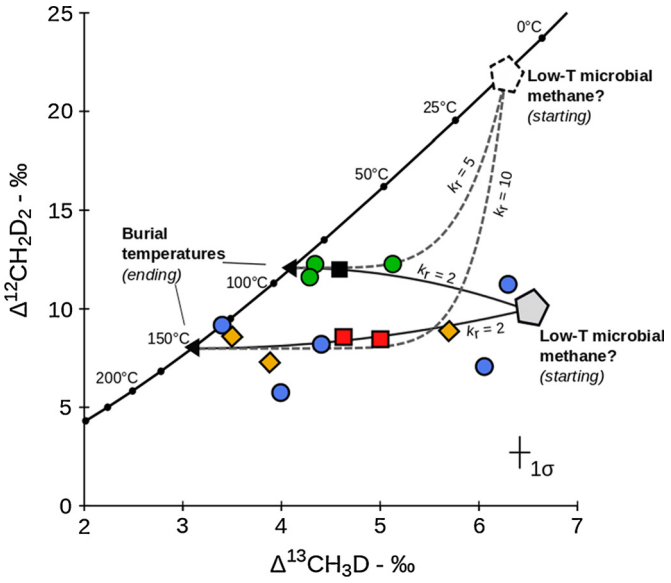

Fig. 7. Exploring the role of different relative rate of re-equilibration. Here we assume that spread to the right of the equilibrium curve reflect partial re-equilibration of $\Delta^{12}CH_2D_2$ and $\Delta^{13}CH_3D$ to burial temperatures of 90 °C and 150 °C. The relative rate is expressed as $k_r = k_{^{12}CH_2D_2}/k_{^{13}CH_3D}$ (or $= k_1/k_2$ in Equations (7) and (8)). If assuming a starting isotopologue composition plotting on the equilibrium curve at an equivalent temperature of ~10 °C (dashed-pentagon symbol), then k_r is required to be at least of 5 to 10 to explain the data (gray dashed arrows). Alternatively, attempting to fit the data with $k_r = 2$, as suggested by ab initio calculations (see Appendices), implies that methane isotopologue signature prior to re-equilibration was plotting out of the equilibrium curve, perhaps with a $\Delta^{12}CH_2D_2$ signature (coincidentally) not too different from equilibrium 'ending' signatures. For illustration, one possible out-of-equilibrium starting composition is reported here (grey-pentagon symbol) that would allow fitting the SoM data with $k_r = 2$.

The form of Equations (7) and (8) show that if the rate constants are the same, and so the e-folding times being $\tau_i = 1/k_i$ are the same, then the relative rates of equilibration depend on the degree of disequilibrium. For example, for an initial gas −50‰ out of equilibrium in $\Delta^{12}CH_2D_2$ and −2‰ out of equilibrium in $^{13}CH_3D$, after $t = 2\tau$, we obtain $\Delta^{12}CH_2D_2 = -7$‰ relative to equilibrium (a total shift of +43‰) and $^{13}CH_3D$ is −0.3‰ relative to equilibrium (a total shift of +1.6‰). So, if the rate constants for D/H exchange, for example, are the same for the two isotopologues, we should see much larger shifts in $^{12}CH_2D_2$ relative to those in $^{13}CH_3D$, but, when the former is at equilibrium, the latter should be also.

We find that unequal rate constants are required to explain our data if the methane prior to re-equilibration was in equilibrium at the lower temperatures suggested by the highest $\Delta^{13}CH_3D$ values. Indeed, for such initial conditions, we calculate that the rate for re-equilibrating $\Delta^{12}CH_2D_2$ would have to be 5 to 10 times that of $\Delta^{13}CH_3D$ to explain a nearly-horizontal relationship as observed in Fig. 7. Whether such large difference of re-equilibration rates between the two isotopologues is likely or not will have to be explored in future experimental work. However, based on an analysis of the rates of equilibration based on the symmetry numbers for reactants and transition states (see Labidi et al., 2020 and Supplementary material), we conclude that one should not expect k_1/k_2 (i.e., the rate constant for $^{12}CH_2D_2$ relative to that for $^{13}CH_3D$) to be not larger than 2. With this constraint, fitting the SoM data suggests that the initial mass-18 isotopologue composition was below the equilibrium curve (Fig. 7). An initial composition such as this for a microbial gas is not unreasonable given the propensity of microbial methanogenesis to produce low $\Delta^{12}CH_2D_2$ values in general, even in some marine environments (e.g., Ash et al., 2019).

6. Implications for the use of methane isotopologues as geothermometers

Three pathways for methane generation (abiotic, thermogenic and microbial) are generally expected to be controlled by kinetic effects rather than by thermodynamic equilibrium. It is thus remarkable that in many instances in nature, especially for thermogenic gases, the 'clumped' composition appears consistent with bond equilibrium. Hence, assessing whether such equilibrium is inherited: 1) from the formation of the methane itself; or 2) from isotopic bond-order re-equilibration under conditions and timescales that remain to be defined, is critical for understanding the true meaning of 'clumped'-based temperatures. In the first case, the 'clumped' composition may accurately record the formation temperature of the methane, whereas in the second case, it is overprinted by a re-equilibration temperature experienced at a point in time in the thermal history of the gas.

We suggest that pristine $\Delta^{13}CH_3D$ and $\Delta^{12}CH_2D_2$ signatures inherited from methane generation, in particular of microbial methanogenesis, have been fully or partially overprinted by re-equilibration within the subsurface of the SoM. This conclusion thus supports the idea that in sedimentary reservoirs, isotopologue equilibrium might sometimes be reached after CH_4 formation. The timescales for re-equilibration remain to be established. Though these rates certainly depend on the associated mineralogy as well as on the presence of H-bearing molecules, they likely scale with temperature (Stolper et al., 2017). This suggests that 'clumped'-based temperatures are more prone to record the highest temperatures experienced by the gases. Considering that thermogenic gases are formed continuously during burial, thus spanning a wide range of temperatures, methane formed at lower temperatures eventually re-equilibrates to the highest temperature reached. This hypothesis would explain why temperatures derived from 'clumped' isotopologues for thermogenic gases often match the maximum burial temperatures (Stolper et al., 2014b, 2017).

On the other hand, data from sedimentary reservoirs in Southwest Ontario and Michigan basins (Giunta et al., 2019) show considerable $\Delta^{12}CH_2D_2$ disequilibrium, illustrating a mixing relationship between thermogenic and microbial methane (see Fig. 4). Those disequilibrium signatures are similar to those observed in laboratory cultures, and suggest that re-equilibration in these reservoirs was limited (if any), thus contrasting with the Marmara system studied here. A possible explanation is that samples from Southwest Ontario and Michigan basins come from sedimentary units that never experienced temperatures greater 40-50 °C. We thus speculate that an activation temperature exists, below which rates for re-equilibration are too slow for significant effects on $\Delta^{13}CH_3D$ and $\Delta^{12}CH_2D_2$ over geological timescales. Identifying threshold temperatures would help define where to expect re-equilibration of microbial methane that is generally formed at lower temperatures than thermogenic gases. From our data, isotopologue equilibrium measured for samples of apparent microbial origin, samples DV05-PE02, DV04-PE04 and PE08, indicates that re-equilibration to temperatures down to 90 °C likely occurs. Not withstanding that re-equilibration rates are likely a function of *in situ* chemical and mineralogical conditions, the contrasting results of these two studies may in turn suggest that a temperature of 40-50 °C is not sufficient for significant re-equilibration of methane isotopic bond ordering.

7. Conclusion

We measured $\Delta^{13}CH_3D$ and $\Delta^{12}CH_2D_2$ from methane-rich cold seeps emanating at the seafloor of the Sea of Marmara (SoM). The variability observed among the samples further demonstrates the occurrence of a multitude of distinct gas reservoirs in the subsurface of the SoM, which is consistent with previous observations based on gas geochemistry (Ruffine et al., 2018b), as well as on seismic imaging (Géli et al., 2018).

Although $\Delta^{13}CH_3D$ and $\Delta^{12}CH_2D_2$ have been recently used to infer the dominant production mechanism (including sometimes, formation temperature) or mixing relationship between different sources of methane (e.g. Giunta et al., 2019), here we show that methane isotopologues signatures in the SoM cannot be simply explained by mixing. Instead, methane effusing from the SoM seafloor appears to be affected, to varying degrees, by bond re-equilibration, a process in which the isotope bond-ordering inherited from the formation of the methane is subsequently 're-set' to thermodynamic equilibrium during residence at sufficiently high temperatures. This conclusion may suggest that apparent isotopologue equilibrium like overwhelmingly displayed among thermogenic gases (Stolper et al., 2015, 2017; Wang et al., 2015; Young et al., 2017; Giunta et al., 2019) can in some cases be acquired after formation and therefore, that isotopologue apparent temperatures may trace re-equilibration temperatures rather than the actual formation temperature.

CRediT authorship contribution statement

LR and **IEK** designed the study. **LR**, **JPD**, **LG**, **MNC**, **HL** collected the samples. **IEK** and **JL** performed the isotopic analyses. **TG** analyzed the data and wrote the manuscript with substantial editing and interpretation inputs from **JL**, **EDY** and **LR**. All authors contributed to final editing of the manuscript.

Declaration of competing interest

The authors declare that they have no known competing financial interests or personal relationships that could have appeared to influence the work reported in this paper.

Acknowledgements

We thank the captain and his crew on-board the RV *Pourquoi pas?* This study was supported by fundings from the European programme "MARsite" under the call ENV.2012.6.4-2, as well as by LabexMER (ANR-10-LABX-19) through the project MicroGaMa. The authors wish to thank Nina Tanguy for providing the bathymetric map. They also thank Dr. David T. Wang, one anonymous reviewer and Dr. Laura Robinson for their helpful comments.

Appendix A. Isotopologue relationship to temperature

The relationship between $\Delta^{13}CH_3D$ and $\Delta^{12}CH_2D_2$ and temperature can be predicted through *ab initio* calculations (e.g. Webb and Miller, 2014). In this study, we used the recent expressions proposed by Young et al. (2016, 2017) (see Table 1):

$$\begin{aligned}&\Delta^{13}CH_3D(T)\\&\approx 1000\ln(1+0.0355502/T-433.038/T^2+1270210.0/T^3\\&\quad-5.94804\times10^8/T^4+1.196630\times10^{11}/T^5\\&\quad-9.07230\times10^{12}/T^6)\end{aligned}\tag{A.1}$$

and

$$\begin{aligned}&\Delta^{12}CH_2D_2(T)\\&\approx 1000\ln(1+0.183798/T-785.483/T^2+1056280.0/T^3\\&\quad+9.37307\times10^7/T^4-8.919480\times10^{10}/T^5\\&\quad+9.901730\times10^{12}/T^6)\end{aligned}\tag{A.2}$$

Table 1
Data for Marmara gas samples. Isotopologue-based temperatures are calculated based on equations in the Appendix. Errors on temperature calculation are 1σ.

Location	Sample	Ruffine et al. (2018b)			Measured on the Panorama (this study)							
		$\delta^{13}C$ (VPDB)	δD (VSMOW)	C_1/C_{2+}	$\delta^{13}C$ (VPDB)	δD (VSMOW)	$\Delta^{13}CH_3D$	T (°C)	±	$\Delta^{12}CH_2D_2$	T (°C)	±
DV1-Central High	DV1-PE02	−43.5	−210	206	−43.3	−207.4	4.59	68.0	4/5	12.00	91.5	9/9
	DV1-PE03	−53	−223	120								
DV2-Western High	DV2-PE01	−44.6	−222	19	−44.6	−220.9	5.00	51.5	4/4	8.47	142	13/15
	DV2-PE02	−44	−229	9	−43.8	−226.1	4.63	66.5	5/5	8.58	140	13/15
DV3-Western flanck Tekirdag	DV3-PE01	−52.3	−214	31	−52.0	−212.3	6.06	16.0	3/3	7.08	169.3	16/19
	DV3-PE02	−57.3	−218	34	n.m	n.m	n.m	n.m		n.m	n.m	
	DV3-PE03	−41.9	−173	10	−41.2	−169.7	3.40	130.5	6/7	9.16	130.3	12/14
	DV3-PE04	−54.8	−216	880	−54.6	−214.0	4.41	76.0	5/5	8.21	146.6	14/15
	DV3-PE06	−52.2	−213	31	−51.9	−210.7	3.99	96.5	6/6	5.77	201.5	21/25
	DV3-PE09	−58.4	−215	1560	−58.0	−214.2	6.30	9.0	3/3	11.25	100.5	10/11
DV4-Southeastern flanck Tekirdag	DV4-PE02	−63.8	−210	5285	−63.8	−208.1	4.29	81.5	5/6	11.61	96	10/10
	DV4-PE07	−66.1	−237	19505	−65.8	−235.6	5.13	46.5	4/4	12.27	88.2	9/10
	DV4-PE08	−66	−243	23147	−65.8	−240.8	4.34	79.5	5/5	12.27	88.2	9/10
DV5-Cinarcik Basin	DV5-PE01	−63.5	−253	1853	−63.3	−252.2	3.89	102.0	6/6	7.29	164.8	16/18
	DV5-PE02	−63.1	−251	1456	−62.9	−248.5	3.50	124.5	7/7	8.61	139.5	14/15
	DV5-PE03	−63.8	−248	12314	−63.7	−249.2	5.70	27.0	3/3	8.89	134.8	13/14
	DV5-PE04	−62.1	−228	1437	n.m	n.m	n.m	n.m		n.m	n.m	

where T is in Kelvin. The differences between the different computational methods to predict relationship between Δ values and temperatures are less than the analytical uncertainties (Webb and Miller, 2014; Young et al., 2016).

Appendix B. Supplementary material

Supplementary material related to this article can be found online at https://doi.org/10.1016/j.epsl.2020.116619.

References

Alexander, R., Kagi, R.I., Larcher, A.V., 1982. Clay catalysis of aromatic hydrogen-exchange reactions. Geochim. Cosmochim. Acta 46 (2), 219–222.

Ambraseys, N.N., Jackson, J.A., 2000. Seismicity of the Sea of Marmara (Turkey) since 1500. Geophys. J. Int. 141 (3), F1–F6.

Armijo, R., Meyer, B., Barka, A., de Chabalier, J.B., Hubert-Ferrari, A., Cakir, Z., 2000. The fault breaks of the 1999 earthquakes in Turkey and the tectonic evolution of the Sea of Marmara: a summary. The 1999 İzmit and Düzce earthquakes: preliminary results, pp. 55–62.

Ash, J., Egger, M., Treude, T., Kohl, I., Cragg, B., Parkes, R.J., et al., 2019. Exchange catalysis during anaerobic methanotrophy revealed by 12CH2D2 and 13CH3D in methane. Geochem. Perspect. Lett. 10, 26–30.

Bernard, B.B., Brooks, J.M., Sackett, W.M., 1976. Natural gas seepage in the Gulf of Mexico. Earth Planet. Sci. Lett. 31 (1), 48–54.

Berner, U., Faber, E., 1996. Empirical carbon isotope/maturity relationships for gases from algal kerogens and terrigenous organic matter, based on dry, open-system pyrolysis. Org. Geochem. 24 (10–11), 947–955.

Bourry, C., Chazallon, B., Charlou, J.L., Donval, J.P., Ruffine, L., Henry, P., et al., 2009. Free gas and gas hydrates from the Sea of Marmara, Turkey: chemical and structural characterization. Chem. Geol. 264 (1–4), 197–206.

Cao, X., Bao, H., Peng, Y., 2019. A kinetic model for isotopologue signatures of methane generated by biotic and abiotic CO2 methanation. Geochim. Cosmochim. Acta 249, 59–75.

Clayton, C., 1991. Carbon isotope fractionation during natural gas generation from kerogen. Mar. Pet. Geol. 8 (2), 232–240.

Crémière, A., Pierre, C., Blanc-Valleron, M.M., Zitter, T., Çağatay, M.N., Henry, P., 2012. Methane-derived authigenic carbonates along the North Anatolian fault system in the Sea of Marmara (Turkey). Deep-Sea Res., Part 1, Oceanogr. Res. Pap. 66, 114–130.

Douglas, P.M.J., Stolper, D.A., Smith, D.A., Anthony, K.W., Paull, C.K., Dallimore, S., et al., 2016. Diverse origins of Arctic and Subarctic methane point source emissions identified with multiply-substituted isotopologues. Geochim. Cosmochim. Acta 188, 163–188.

Eldridge, D.L., Korol, R., Lloyd, M.K., Turner, A.C., Webb, M.A., Miller, T.F., Stolper, D., 2019. Comparison of experimental vs. theoretical abundances of 13CH3D and 12CH2D2 for isotopically equilibrated systems from 1-500 °C. ACS Earth Space Chem. 3 (12), 2747–2764.

Gasperini, L., Polonia, A., Bortoluzzi, G., Henry, P., Le Pichon, X., Tryon, M., Cagatay, N., Geli, L., 2011. How far did the surface rupture of the 1999 Izmit earthquake reach in Sea of Marmara? Tectonics 30.

Géli, L., Henry, P., Zitter, T., Dupré, S., Tryon, M., Çağatay, M.N., et al., 2008. Gas emissions and active tectonics within the submerged section of the North Anatolian Fault zone in the Sea of Marmara. Earth Planet. Sci. Lett. 274 (1–2), 34–39.

Géli, L., Henry, P., Grall, C., Tary, J.B., Lomax, A., Batsi, E., et al., 2018. Gas and seismicity within the Istanbul seismic gap. Sci. Rep. 8 (1), 6819.

Giunta, T., Young, E.D., Warr, O., Kohl, I., Ash, J.L., Martini, A., et al., 2019. Methane sources and sinks in continental sedimentary systems: new insights from paired clumped isotopologues 13CH3D and 12CH2D2. Geochim. Cosmochim. Acta 245, 327–351.

Gonzalez, Y., Nelson, D.D., Shorter, J.H., McManus, J.B., Dyroff, C., Formolo, M., Wang, D.T., Western, C.M., Ono, S., 2019. Precise measurements of 12CH2D2 by tunable infrared laser direct absorption spectroscopy. Anal. Chem. 91 (23), 14967–14974.

Gruen, D.S., Wang, D.T., Könneke, M., Topçuoğlu, B.D., Stewart, L.C., Goldhammer, T., et al., 2018. Experimental investigation on the controls of clumped isotopologue and hydrogen isotope ratios in microbial methane. Geochim. Cosmochim. Acta 237, 339–356.

Gürgey, K., 2009. Geochemical overview and undiscovered gas resources generated from Hamitabat petroleum system in the Thrace Basin, Turkey. Mar. Pet. Geol. 26 (7), 1240–1254.

Gürgey, K., Philp, R., Clayton, C., Emiro lu, H., Siyako, M., 2005. Geochemical and isotopic approach to maturity/source/mixing estimations for natural gas and associated condensates in the Thrace Basin, NW Turkey. Appl. Geochem. 20 (11), 2017–2037.

Huvaz, O., Sarikaya, H., Nohut, O.M., 2005. Nature of a regional dogleg pattern in maturity profiles from Thrace basin, northwestern Turkey: A newly discovered unconformity or a thermal anomaly? AAPG Bull. 89 (10), 1373–1396.

Head, I.M., Jones, D.M., Larter, S.R., 2003. Biological activity in the deep subsurface and the origin of heavy oil. Nature 426 (6964), 344.

Holler, T., Widdel, F., Knittel, K., Amann, R., Kellermann, M.Y., Hinrichs, K.U., et al., 2011. Thermophilic anaerobic oxidation of methane by marine microbial consortia. ISME J. 5 (12), 1946–1956.

Horibe, Y., Craig, H., 1995. DH fractionation in the system methane-hydrogen-water. Geochim. Cosmochim. Acta 59 (24), 5209–5217.

Inagaki, F., Hinrichs, K.U., Kubo, Y., Bowles, M.W., Heuer, V.B., Hong, W.L., et al., 2015. Exploring deep microbial life in coal-bearing sediment down to ∼2.5 km below the ocean floor. Science 349 (6246), 420–424.

James, A.T., Burns, B.J., 1984. Microbial alteration of subsurface natural gas accumulations. AAPG Bull. 68 (8), 957–960.

Kashefi, K., Lovley, D.R., 2003. Extending the upper temperature limit for life. Science 301 (5635), 934.

Labidi, J., Young, E.D., Giunta, T., Kohl, I.E., Seewald, J., Tang, H., et al., 2020. Methane thermometry in deep-sea hydrothermal systems: evidence for re-ordering of doubly-substituted isotopologues during fluid cooling. Geochim. Cosmochim. Acta 288, 248–261.

Luff, R., Wallmann, K., 2003. Fluid flow, methane fluxes, carbonate precipitation and biogeochemical turnover in gas hydrate-bearing sediments at Hydrate Ridge, Cascadia Margin: numerical modeling and mass balances. Geochim. Cosmochim. Acta 67 (18), 3403–3421.

Martini, A.M., Walter, L.M., Budai, J.M., Ku, T.C., Kaiser, C.J., Schoell, M., 1998. Genetic and temporal relations between formation waters and biogenic methane: Upper Devonian Antrim Shale, Michigan Basin, USA. Geochim. Cosmochim. Acta 62 (10), 1699–1720.

McCollom, T.M., 2013. Laboratory simulations of abiotic hydrocarbon formation in Earth's deep subsurface. Rev. Mineral. Geochem. 75 (1), 467–494.

Ono, S., Wang, D.T., Gruen, D.S., Sherwood Lollar, B., Zahniser, M.S., McManus, B.J., Nelson, D.D., 2014. Measurement of a doubly substituted methane isotopologue, 13CH3D, by tunable infrared laser direct absorption spectroscopy. Anal. Chem. 86 (13), 6487–6494.

Prinzhofer, A., Pernaton, E., 1997. Isotopically light methane in natural gas: bacterial imprint or diffusive fractionation? Chem. Geol. 142 (3–4), 193–200.

Richter, F.M., Mendybaev, R.A., Christensen, J.N., Hutcheon, I.D., Williams, R.W., Sturchio, N.C., Beloso Jr, A.D., 2006. Kinetic isotopic fractionation during diffusion of ionic species in water. Geochim. Cosmochim. Acta 70 (2), 277–289.

Ruffine, L., Dennielou, B., Giovanni, B., Namik, Ç.M., Grall, C., Jean-Luc, C., et al., 2012. Geochemical Dynamics of the Natural-Gas Hydrate System in the Sea of Marmara, Offshore Turkey. INTECH Open Access Publisher.

Ruffine, L., Germain, Y., Polonia, A., de Prunelé, A., Croguennec, C., Donval, J.P., et al., 2015. Pore water geochemistry at two seismogenic areas in the Sea of Marmara. Geochem. Geophys. Geosyst. 16 (7), 2038–2057.

Ruffine, L., Donval, J.P., Croguennec, C., Burnard, P., Lu, H., Germain, Y., et al., 2018b. Multiple gas reservoirs are responsible for the gas emissions along the Marmara fault network. Deep-Sea Res., Part 2, Top. Stud. Oceanogr. 153, 48–60.

Ruffine, L., Ondreas, H., Blanc-Valleron, M.M., Teichert, B.M., Scalabrin, C., Rinnert, E., et al., 2018a. Multidisciplinary investigation on cold seeps with vigorous gas emissions in the Sea of Marmara (MarsiteCruise): strategy for site detection and sampling and first scientific outcome. Deep-Sea Res., Part 2, Top. Stud. Oceanogr. 153, 36–47.

Sattler, A., 2018. Hydrogen/deuterium (H/D) exchange catalysis in alkanes. ACS Catal. 8 (3), 2296–2312.

Schoell, M., 1988. Multiple origins of methane in the Earth. Chem. Geol. 71 (1–3), 1–10.

Sessions, A.L., Sylva, S.P., Summons, R.E., Hayes, J.M., 2004. Isotopic exchange of carbon-bound hydrogen over geologic timescales. Geochim. Cosmochim. Acta 68, 1545–1559.

Shuai, Y., Douglas, P.M., Zhang, S., Stolper, D.A., Ellis, G.S., Lawson, M., et al., 2018. Equilibrium and non-equilibrium controls on the abundances of clumped isotopologues of methane during thermogenic formation in laboratory experiments: implications for the chemistry of pyrolysis and the origins of natural gases. Geochim. Cosmochim. Acta 223, 159–174.

Stolper, D.A., Lawson, M., Davis, C.L., Ferreira, A.A., Neto, E.S., Ellis, G.S., et al., 2014b. Formation temperatures of thermogenic and biogenic methane. Science 344 (6191), 1500–1503.

Stolper, D.A., Sessions, A.L., Ferreira, A.A., Neto, E.S., Schimmelmann, A., Shusta, S.S., et al., 2014a. Combined 13 C–D and D–D clumping in methane: methods and preliminary results. Geochim. Cosmochim. Acta 126, 169–191.

Stolper, D.A., Martini, A.M., Clog, M., Douglas, P.M., Shusta, S.S., Valentine, D.L., et al., 2015. Distinguishing and understanding thermogenic and biogenic sources of methane using multiply substituted isotopologues. Geochim. Cosmochim. Acta 161, 219–247.

Stolper, D.A., Lawson, M., Formolo, M.J., Davis, C.L., Douglas, P.M., Eiler, J.M., 2017. The utility of methane clumped isotopes to constrain the origins of methane in natural gas accumulations. Geol. Soc. (Lond.) Spec. Publ. 468. SP468-3.

Taenzer, L., Labidi, J., Masterson, A.L., Feng, X., Rumble III, D., Young, E.D., Leavitt, W.D., 2020. Low Δ12CH2D2 values in microbialgenic methane result from combinatorial isotope effects. Geochim. Cosmochim. Acta 285, 225–236.

Takai, K., Nakamura, K., Toki, T., Tsunogai, U., Miyazaki, M., Miyazaki, J., et al., 2008. Cell proliferation at 122 C and isotopically heavy CH4 production by a hyperthermophilic methanogen under high-pressure cultivation. Proc. Natl. Acad. Sci. 105 (31), 10949–10954.

Tang, Y., Perry, J.K., Jenden, P.D., Schoell, M., 2000. Mathematical modeling of stable carbon isotope ratios in natural gases. Geochim. Cosmochim. Acta 64 (15), 2673–2687.

Teichert, B.M.A., Chevalier, N., Gussone, N., Bayon, G., Ponzevera, E., Ruffine, L., Strauss, H., 2018. Sulfate-dependent anaerobic oxidation of methane at a highly dynamic bubbling site in the Eastern Sea of Marmara (Çinarcik Basin). Deep-Sea Res., Part 2, Top. Stud. Oceanogr. 153, 79–91.

Tissot, B., Welte, D.H., 1978. Petroleum Occurrence and Formation.

Treude, T., Boetius, A., Knittel, K., Wallmann, K., Jørgensen, B.B., 2003. Anaerobic oxidation of methane above gas hydrates at Hydrate Ridge, NE Pacific Ocean. Mar. Ecol. Prog. Ser. 264, 1–14.

Wang, D.T., Gruen, D.S., Sherwood Lollar, B., Hinrichs, K.U., Stewart, L.C., Holden, J.F., et al., 2015. Nonequilibrium clumped isotope signals in microbial methane. Science 348 (6233), 428–431.

Wang, D.T., Reeves, E.P., McDermott, J.M., Seewald, J.S., Ono, S., 2018. Clumped isotopologue constraints on the origin of methane at seafloor hot springs. Geochim. Cosmochim. Acta 223, 141–158.

Wang, Z., Schauble, E.A., Eiler, J.M., 2004. Equilibrium thermodynamics of multiply substituted isotopologues of molecular gases. Geochim. Cosmochim. Acta 68 (23), 4779–4797.

Webb, M.A., Miller III, T.F., 2014. Position-specific and clumped stable isotope studies: comparison of the Urey and path-integral approaches for carbon dioxide, nitrous oxide, methane, and propane. J. Phys. Chem. A 118 (2), 467–474.

Whiticar, M.J., 1999. Carbon and hydrogen isotope systematics of bacterial formation and oxidation of methane. Chem. Geol. 161 (1–3), 291–314.

Xia, X., Gao, Y., 2019. Kinetic clumped isotope fractionation during the thermal generation and hydrogen exchange of methane. Geochim. Cosmochim. Acta 248, 252–273.

Yoshinaga, M.Y., Holler, T., Goldhammer, T., Wegener, G., Pohlman, J.W., Brunner, B., et al., 2014. Carbon isotope equilibration during sulphate-limited anaerobic oxidation of methane. Nat. Geosci. 7 (3), 190–194.

Young, E.D., 2019. A two-dimensional perspective on CH4 isotope clumping. Deep Carbon: Past to Present, 388–414.

Young, E.D., Rumble III, D., Freedman, P., Mills, M., 2016. A large-radius high-mass-resolution multiple-collector isotope ratio mass spectrometer for analysis of rare isotopologues of O2, N2, CH4 and other gases. Int. J. Mass Spectrom. 401, 1–10.

Young, E.D., Kohl, I.E., Lollar, B.S., Etiope, G., Rumble Iii, D., Li, S., et al., 2017. The relative abundances of resolved l2CH2D2 and 13CH3D and mechanisms controlling isotopic bond ordering in abiotic and biotic methane gases. Geochim. Cosmochim. Acta 203, 235–264.